Molecular Dynamics Simulations of Classical Sound Absorption in a Monatomic Gas

M. Ayub,[1, a)] A. C. Zander,[1] D. M. Huang,[2] B. S. Cazzolato,[1] and C. Q. Howard[1]

[1)] *The University of Adelaide, School of Mechanical Engineering, Adelaide, SA 5005, Australia*

[2)] *The University of Adelaide, School of Physical Sciences, Department of Chemistry, Adelaide, SA 5005, Australia*

(Dated: 29 January 2018)

Sound wave propagation in argon gas is simulated using molecular dynamics (MD) in order to determine the attenuation of acoustic energy due to classical (viscous and thermal) losses at high frequencies. In addition, a method is described to estimate attenuation of acoustic energy using the thermodynamic concept of exergy. The results are compared against standing wave theory and the predictions of the theory of continuum mechanics. Acoustic energy losses are studied by evaluating various attenuation parameters and by comparing the changes in behavior at three different frequencies. This study demonstrates acoustic absorption effects in a gas simulated in a thermostatted-molecular simulation and quantifies the classical losses in terms of the sound attenuation constant. The approach can be extended to further understanding of acoustic loss mechanisms in the presence of nanoscale porous materials in the simulation domain.

PACS numbers: 82.20.Wt, 83.10.Mj, 83.10.Rs, 43.20.Bi, 43.20.Hq, 05.70.Ce

Keywords: Molecular dynamics, classical sound absorption, viscous and thermal losses, sound attenuation, and themoacoustic exergy concepts.

[a)]Electronic mail: md.ayub@adelaide.edu.au

I. INTRODUCTION

Nanomaterials show promise as sound-absorbing materials for noise control in applications such as engines, buildings, vehicles, aircraft, spacecraft and watercraft[1–7]. However, the absorption mechanisms of nanoscopic fibers are not fully understood and the application of numerical and analytical modeling methods to this problem is still at an early stage. Although the mechanisms of sound absorption are currently well understood for conventional porous acoustic materials having particle diameters or pores at the microscale (down to 1 μm), the relative influence of the various mechanisms is expected to change for materials with pores or fibers at the smaller nanoscale (down to 1 nm) where other mechanisms and non-linear effects may also have a significant influence. Therefore, modeling acoustic mechanisms at the nanoscale requires molecular simulations that can model the flow behavior in the transition regime[8,9], because the characteristic length scale of the nanoscale structures is comparable to the molecular mean free path, and hence the commonly used acoustic assumptions, such as continuity, are invalid[10]. Molecular simulations such as molecular dynamics (MD) can play an important role in shedding light on the detailed mechanisms by which nanomaterials absorb sound[10–12]. However, conventional molecular dynamics simulation technique assume some conserved quantity and thus it is not straightforward to measure dissipation of acoustic energy. Thus, a need exists for a method to quantify attenuation of acoustic energy during sound wave propagation in a medium (gas) that allows absorption to be modeled in a thermostatted molecular dynamics simulation. Attenuation of sound occurs in a monatomic gas due to viscous and thermal losses (also known as classical losses) of acoustic energy. Viscous losses occur due to the differences in relative motions between adjacent portions of the medium such as during the compression and expansion of the medium that accompany the transmission of an acoustic wave[13]. Thermal losses result from heat conduction between adjacent portions of the medium generated by higher temperature condensations and lower temperature rarefactions. A detailed description of such loss mechanisms can be found in the literature[13,14]. In many situations, especially at low frequency, acoustic dissipation is insignificant and can be ignored for the length and time scales of interest[13]. However, with high-frequency sound wave propagation, the losses are significant for distances on the order of a wavelength. Hence, estimation of losses in a medium for high-frequency sound waves is very important to distinguish between the losses

that occur in the fluid and the losses that occur due to the interaction between the fluid and any other components (for example, absorptive media). Here, a simulation framework for molecular dynamics was developed to study the sound field characteristics of high-frequency wave propagation in a simple gas with the long term aim of extending the study to investigate the absorption behavior of nanomaterials. As such, in this study, MD simulations were performed for an acoustic system consisting of a monatomic gas that accounts for the effects of classical absorption in high-frequency sound propagation, in which losses occur due to the conversion of the coherent acoustic energy into random thermal energy as the wave propagates. A noble contribution of this paper is the use of the thermoacoustic concept of exergy to identify acoustic damping in MD simulations. Exergy is a form of energy that accounts for the ability to do useful work in a system in the presence of a freely accessible thermal reservoir at a particular temperature[15]. A method using the thermoacoustic concept of exergy is demonstrated to distinguish between the coherent acoustic energy and random thermal energy, in which the losses/dissipation of acoustic energy are defined in terms of entropy generation. Estimates of the losses were compared with those of the classical mechanics and standing wave theory for three different frequencies.

In conventional computer simulations of acoustic wave propagation (such as Computational Fluid Dynamics), classical losses are defined using continuum theory and the losses are quantified as a function of sound attenuation based on continuum fluid assumptions[16,17]. As mentioned earlier, the classical sources of attenuation in a sound wave are internal viscous friction and heat conduction. The losses of energy caused by internal friction are determined by the transmitted energy (which is proportional to ρv^2, where v is the particle velocity) and the kinematic viscosity μ/ρ (where μ and ρ are the dynamic viscosity and density of the gas, respectively)[18]. The thermal losses caused by heat conduction are determined by the thermal conductivity κ of the propagation medium and the generated temperature gradient ∇T (where T is the gas temperature) between the hotter (condensed) and cooler (rarefied) regions of the waves[13,14]. The equation for the rate of energy loss in a volume element can be derived from the classical theory of Navier-Stokes and its extension to the Burnett and super-Burnett limits for an acoustic field in terms of an attenuation constant, which is proportional to the square of the frequency[8,13,14,18,19]. However, the theoretical approximations of attenuation for an acoustic system based on a fluid continuum are only applicable at low frequencies, where the relaxation time for absorption (viscous and thermal) is similar to

the mean time between collisions[10,13]. Thus, for frequencies approaching the relaxation frequency, where the wavelength is about the same size as the mean free path, the assumption of fluid continuum is inaccurate[10,13]. Hence, the classical theory is not applicable for high-frequency wave propagation or nanoscale systems for which the characteristic length scale is comparable to the molecular mean free path. As such, classical losses estimated based on the theory of continuum mechanics may not be applicable for evaluating attenuation in molecular dynamics simulations of acoustic wave propagation in a gas at the nanoscale. Hadjiconstantinou and Garcia[8] conducted DSMC (Direct Simulation Monte Carlo) simulations of sound wave propagation in the gigahertz (GHz) range. They derived the sound speed and attenuation coefficient by non-linear fitting the simulation results of velocity amplitude, assuming plane-wave theory. It was observed that the predictions were significantly affected by the free molecular flow near the sound source in a high-frequency sound wave propagation, where the wavelength was comparable to the mean free path. Thus, the curve fits of the waveforms indicated the sensitivity of the results to the choice of the distance for data fits from the sound source[8]. Therefore, it is important to have a method that can accurately measure losses due to classical acoustic-absorption mechanisms in a nanoscale domain for high-frequencies, without relying on factors such as free molecular flow or continuum approximations[10,12]. Hence a comprehensive method is developed here based on entropy generation.

This paper is organized as follows. First, Section II describes the simulation domain and simulation parameters required to model the sound wave propagation. Second, Section III presents the development of the relevant theories and modified calculation methods that were used to obtain sound attenuation parameters of the simulated wave. Finally, the simulation results are discussed in Section IV. The deviations from classical mechanics are also discussed in this section. Overall, this paper demonstrates the utility of the MD simulation method to study classical acoustic absorption in a simple gas at the nanoscale.

II. SIMULATION DETAILS

A rectangular domain of length $L_z = 150\,\text{nm}$ in the wave propagation direction shown in Figure 1 was used to simulate plane sound wave propagating in a monatomic gas (argon). The simulation domain had dimensions of $L_x = L_y = 70\,\text{nm}$ transverse to the wave prop-

agation direction. The simulation domain was chosen for high-frequency sound-wave propagation at a frequency of $f \approx 1.5\,\mathrm{GHz}$, with a domain length equivalent to approximately half the wavelength of the acoustic wave to reduce computational cost without sacrificing the accuracy of the simulation results. Molecular dynamics simulations were performed at frequencies of $f \approx 1.5$, 2 and $2.5\,\mathrm{GHz}$ to enable observations of the changes in the sound field as the excitation frequency changed. It should be clarified that the flow regimes of the simulated waves are in the transition regime ($0.1<Kn<10$)[8,9], as the Knudsen number measuring the ratio of the molecular mean free path ($\lambda_{\mathrm{mfp}}=7.28\times10^{-8}$ m) to the characteristic length scale (H, in this case the acoustic wave length, λ) is $Kn=\frac{\lambda_{\mathrm{mfp}}}{H}\approx 0.25$, 0.34, and 0.42 for the simulated frequencies of $f \approx 1.5$, 2 and $2.5\,\mathrm{GHz}$, respectively.

The large-scale atomic/molecular massively parallel simulator (LAMMPS) package[20,21] was used for the simulations. An oscillating wall comprising a closed packed FCC (Face-Centered Cubic) lattice of "solid" argon atoms was used as a sound source and excited at $z = 0$ by imposing a sinusoidally varying velocity in the positive z-direction. Figure 1(a) shows a sketch of the simulation domain, where the far end of the simulation domain in the z-direction was terminated with a specular reflecting wall and the system was replicated in the transverse directions using periodic boundary conditions. The domain was filled with argon gas with a density of $\rho = 1.8\,\mathrm{kg\,m^{-3}}$ (20,412 molecules) to maintain the gas pressure at $P = 1\,\mathrm{atm}$.

In the simulations at high frequency, an auxiliary mechanism that is compatible with wave propagation modeling was required to remove the additional heat from the system, in where the rapid oscillation of the sound source heats the system rapidly as the acoustic source continuously does work on the gas. Therefore, a Nosé-Hoover thermostat at $T = 273\,\mathrm{K}$ was coupled loosely (with a thermostatting damping time (τ) of 1 period) to the degrees of freedom of the gas molecules perpendicular (x and y) to the propagating wave (z-direction) to control the temperature[11]. The piston wall of solid argon, combined with the thermostat applied on the gas, was designed to mimic a diffuse reflection boundary condition. The wall was created by holding a collection of 35,645 argon atoms fixed with respect to one another. The oscillation of the wall was generated with a velocity assigned to wall atoms collectively by imposing a sinusoidally varying velocity in the z-direction. During the simulation, the piston created the sinusoidally varying velocity while the thermostat imposed a Maxwellian-Boltzmann distribution at the desired temperature on the velocity components of the gas

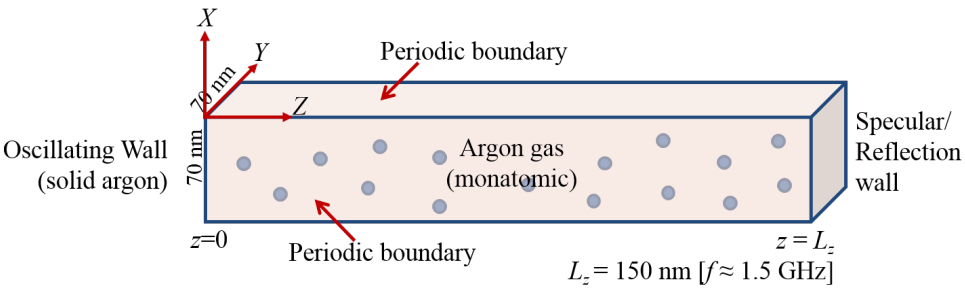

(a)

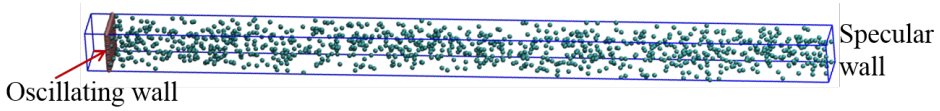

(b)

FIG. 1. Schematic (a) and snapshot (b) of MD simulation domain and sound source model for acoustic wave propagation in argon gas.

molecules perpendicular to the wave propagation direction.

The interactions between gas molecules (i.e., argon-argon) was described by a Lennard-Jones (LJ) 12-6 potential with LJ parameters $\varepsilon_{ij} = 10.33$ meV and $\sigma_{ij} = 3.40$ Å and a cut-off distance of $3\sigma_{ij}$[22]. A short-range purely repulsive WCA (Weeks-Chandler-Andersen) potential[23] with the same LJ parameters was used for the interaction between the atoms of the solid wall and those of the propagating medium (gas) by truncating the LJ potential at $2^{\frac{1}{6}}\,\sigma_{ij}$.

Simulations were initiated with a Maxwell-Boltzmann distribution of gas velocities corresponding to a temperature of $T = 273\,\mathrm{K}$ and were equilibrated for 2 ns at the same temperature of $T = 273\,\mathrm{K}$ with the piston stationary. A Langevin thermostat was used to control the gas temperature during the equilibration period. Thereafter, the temperature was maintained with a Nosé-Hoover thermostat and further relaxed for 750 ps at the same temperature. Then, the piston was sinusoidally oscillated at a frequency of approximately 1.5 GHz with a velocity of $v_0 = 0.15c = 49.69\,\mathrm{m\,s^{-1}}$ to excite the system with an acoustic wave. A timestep size of 0.5 fs was used during the equilibration of the gas and a 1 fs timestep was used during the wave propagation period. The simulation was run for nearly 67.5 ns, which was equivalent to 100 periods of the propagating wave cycle. To extract sound propagation data, sampling was done during the final 40 periods of the simulation, with 60 spatial

bins (three-dimensional microscopic boxes of atoms) per wavelength. Furthermore, it should also be reemphasized that at the high frequency considered, i.e. $f \approx 1.5\,\mathrm{GHz}$, simulations were performed with a large initial velocity amplitude of $v_0 = 0.15c$ due to the considerable attenuation observed at such a high frequency. However, even under these conditions, v_0 was small compared with the most probable molecular velocity c_m of the gas, which usually has the same order as the sound speed c.

By monitoring the global temperature, pressure, kinetic energy and potential energy and spatial variations along the z-direction of the velocity, density, temperature and pressure as a function of time, it was ascertained that the system had reached equilibrium within 2.5 ns. It was also confirmed that the distribution of gas velocities was Maxwell-Boltzmann in form for the specified temperature under these conditions. The MD simulation framework used here was validated by the authors in a previous publication[11] comparing Hadjiconstantinou and Garcia's[8] results from DSMC simulations, which showed comparable particle velocity amplitudes in the simulation domain.

III. THEORY

A. Attenuation from Total Power and Exergy

In a thermostatted molecular dynamics simulation system, the dissipated energy is converted to the random internal energy of the gas. Thus, keeping track of the conversion of coherent forms of energy into random forms of energy is a convenient way to estimate the losses occurring in the fluid medium. In order to estimate and demonstrate dissipation of acoustic power in the simulation domain due to classical losses in the fluid medium, the estimate of total power flowing in the system is useful for power balance of the system[24]. The total power flowing in the wave-propagation direction can be related to the enthalpy in a moving gas using Rott's acoustic approximation[24], which gives the total power flux in this (z) direction as

$$\dot{H}(z) = \frac{1}{2}\rho \int Re[hv^*]dA - (A\kappa + A_\mathrm{solid}\kappa_\mathrm{solid})\frac{\mathrm{d}T_\mathrm{m}}{\mathrm{d}z}, \tag{1}$$

where h ($= U + PV = E_\mathrm{k} + E_\mathrm{p} + P/\rho$) is the enthalpy per unit mass, v^* is the complex conjugate of the particle velocity v, κ is the thermal conductivity, A is the cross-sectional area, T_m is the mean temperature of the gas and the subscript 'solid' denotes the properties

corresponding to whatever solid is present in the system. The first term on the right side of Equation (1) is the time-averaged enthalpy flux and the second term is the conduction of heat both in the gas and in the solid present in the system. Here, U is the sum of the total kinetic (E_k) and potential (E_p) energy, P is the pressure and V is the volume of the gas.

In order to present the power balance of the model and to estimate the total losses in the system, the concepts demonstrated by Swift[15] for thermoacoustic engines and refrigerators based on the thermodynamics of efficiency are employed. Similar to the method of accounting for efficiency in a complex thermodynamic system, all losses can be measured in terms of equivalent lost work, where a temperature T_0 is identified as the temperature of the environment at which arbitrary amounts of waste heat can be freely exchanged[15]. The lost work (in terms of power) is expressed as the product of the temperature of the environment and the sum of all the entropy generated in the system due to irreversible processes that accompany the operation of the thermoacoustic system[15],

$$\dot{W}_\mathrm{lost} = T_0 \sum \dot{S}_\mathrm{gen}, \tag{2}$$

which is known as the Gouy-Stodola theorem[25]. Here, $\sum \dot{S}_\mathrm{gen}$ is the time-averaged entropy generation rate, expressed as an integral of the instantaneous rate of entropy generation over time and over the entire volume of the apparatus[15]

$$\sum \dot{S}_\mathrm{gen} = \frac{\omega}{2\pi} \int_0^{\frac{2\pi}{\omega}} \int_V \rho \dot{s}_\mathrm{gen} \, \mathrm{d}V \mathrm{d}t, \tag{3}$$

where ω is the angular frequency and $\rho \dot{s}_\mathrm{gen}$ is the instantaneous rate of entropy generation per unit volume, which is the sum of effects from various dissipative processes such as viscous, thermal, frictional and chemical ones involved in loss mechanisms responsible for irreversibility in a thermoacoustic system[15].

Our interpretation of losses was developed from a derivation of an acoustic approximation leading to the Gouy-Stodola theorem[15,25] and from the concept of exergy. The exergy is the maximum amount of work that a system can do as it comes to equilibrium with a thermal reservoir. A brief description of the derivation of an expression for the exergy, which is as described by Swift[15], is presented here. A generalized portion of the simulated system, as shown in the schematic in Figure 2, is considered. For the steady state of the portion shown in Figure 2, the difference between energy fluxes leaving and entering must be zero,

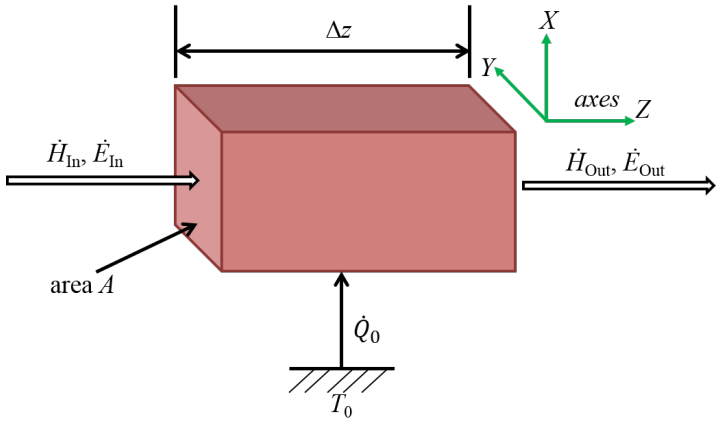

FIG. 2. Schematic of a generalized microscopic portion of the simulation domain of the modeled acoustic system. The wave is propagating in the z-direction and the representative microscopic portion of the simulation domain with length Δz has acoustic power $\dot{E}$ and total power $\dot{H}$ flowing into and out of the left and right open end, respectively. In between the process, the system rejects (or absorbs) thermal power $\dot{Q}_0$ to ambient at T_0. The schematic is adapted from Swift[15].

according to the First Law of Thermodynamics, which can be written as[15]

$$0 = \dot{H}_{\mathrm{Out}} - \dot{H}_{\mathrm{In}} - \dot{Q}_0. \tag{4}$$

Similarly according to the Second Law of Thermodynamics, the entropy generated within the portion must equal to the difference between the entropy fluxes leaving and entering, which can be written as[15]

$$\sum \dot{S}_{\mathrm{gen}} = \frac{\dot{H}_{\mathrm{Out}} - \dot{E}_{\mathrm{Out}}}{T_{\mathrm{mOut}}} - \frac{\dot{H}_{\mathrm{In}} - \dot{E}_{\mathrm{In}}}{T_{\mathrm{mIn}}} - \frac{\dot{Q}_0}{T_0}, \tag{5}$$

where $\dot{E}$ is the acoustic power flowing at a mean temperature T_{m} along the wave path, which is equal to active acoustic intensity I_{ac} when presented as an acoustic power flowing per unit area in a plane wave propagation and $\frac{\dot{H}-\dot{E}}{T_m}$ is the second-order entropy flux. The active acoustic intensity I_{ac} can be associated with the particle velocity, $v(z, f)$, and sound pressure, $p(z, f)$, of the standing wave as[26]

$$I_{\mathrm{ac}} = \frac{1}{2}\mathrm{Re}[pv^*]. \tag{6}$$

Here, v^* is the complex conjugate of the particle velocity $v(z, f)$. To estimate the active intensity from the simulation data, the power spectrum of the cross-correlation between the

sound pressure and particle velocity can be used as[27]

$$I_{\mathrm{ac}} = \mathrm{Re}(G_{\mathrm{pv}}), \tag{7}$$

where G_{pv} is the single-sided cross-power spectral density of the sound pressure and particle velocity. Combining Equations (4) and (5) to eliminate $\dot{Q}_0$ yields[15]

$$\begin{aligned} T_0 \sum \dot{S}_{\mathrm{gen}} = {} & \frac{T_0}{T_{\mathrm{mIn}}} \dot{E}_{\mathrm{In}} + \left(1 - \frac{T_0}{T_{\mathrm{mIn}}}\right) \dot{H}_{\mathrm{In}} \\ & - \frac{T_0}{T_{\mathrm{mOut}}} \dot{E}_{\mathrm{Out}} - \left(1 - \frac{T_0}{T_{\mathrm{mOut}}}\right) \dot{H}_{\mathrm{Out}}, \end{aligned} \tag{8}$$

which can be written in terms of the exergy as

$$T_0 \sum \dot{S}_{\mathrm{gen}} = \dot{X}_{\mathrm{In}} - \dot{X}_{\mathrm{Out}}, \tag{9}$$

with $\dot{X}(z)$ being the time-averaged exergy flux in the z-direction in the simulation domain. The exergy flux $\dot{X}(z)$ can be written as[15]

$$\dot{X} = \frac{T_0}{T_{\mathrm{m}}} \dot{E} + \left(1 - \frac{T_0}{T_{\mathrm{m}}}\right) \dot{H}. \tag{10}$$

The Equation (10) for exergy flux $\dot{X}$ denotes the associated power to do work in the presence of a thermal reservoir at T_0[15]. Expressing $\dot{X}_{\mathrm{In}} = \dot{X}^i$ and $\dot{X}_{\mathrm{Out}} = \dot{X}^{i+1}$, where $i(= 1, 2, 3 \cdots M)$ is the bin number index along the wave propagation direction, and presenting the difference between the exergy flux $(\dot{X}_{\mathrm{In}} - \dot{X}_{\mathrm{Out}})$ as the change in exergy flux in two consecutive bins in the simulation domain, Equation (9) can be written as

$$T_0 \frac{\mathrm{d} \sum \dot{S}_{\mathrm{gen}}}{\mathrm{d}z} = \lim_{\Delta z \to 0} - \frac{\dot{X}^{i+1} - \dot{X}^i}{\Delta z} = - \frac{\mathrm{d}\dot{X}}{\mathrm{d}z}, \tag{11}$$

From Equation (11), it can be seen that work lost and entropy generation can be related in a simple way, when $T_{\mathrm{m}} = T_0$, as[15]

$$- \frac{\mathrm{d}\dot{X}}{\mathrm{d}z} = T_0 \frac{\mathrm{d} \sum \dot{S}_{\mathrm{gen}}}{\mathrm{d}z} = - \frac{\mathrm{d}\dot{E}}{\mathrm{d}z}, \tag{12}$$

which indicates the losses as the dissipation of acoustic power per unit length in a channel along the wave path. In this study, the thermostat was considered as the environment to which waste heat was transferred at $T_0 = T_{\mathrm{thermostat}} = 273\,\mathrm{K}$, which is equivalent to the equilibrium gas temperature of the whole system, and $T_{\mathrm{m}}(z) = \langle T_i \rangle$ is the mean gas temperature of each microscopic bin along the z-direction.

The entropy generation calculated using Equation (11) gives the rate of energy lost per unit length of the microscopic portion of the thermoacoustic system. For a simulation domain of a thermoacoustic system with plane-wave propagation in a volume V, cross-sectional area A and wavelength $\lambda = \frac{2\pi}{k}$, wavenumber k, the rate at which the energy is lost from the wave can be obtained by integrating Equation (11) over the volume[13]. It can be written per unit volume as

$$\frac{\dot{W}_{\text{lost}}}{V} = -\frac{1}{V}\int_0^{\lambda} \nabla \dot{X} \, \mathrm{d}z. \tag{13}$$

Equation (13) gives the power lost per unit volume, which can then be used to obtain the attenuation coefficient m_{e} as,

$$m_{\text{e}} = -\frac{\left[\frac{1}{V}\int_0^{\lambda} \nabla \dot{X} \, \mathrm{d}z\right]}{2I}, \tag{14}$$

where $I(= \frac{1}{2}\rho c v_0^2)$ is the classical acoustic intensity for the simulated wave, $v_0 = 49.69\,\mathrm{m\,s^{-1}}$ is the particle velocity amplitude chosen for the study and subscript 'e' is used to indicate estimation based on the exergy.

In a thermostatted molecular simulation domain, the coherent energy contained in an acoustic wave is transferred to atoms at random times via the stochastic nature of the interactions of atoms as the wave propagates, which leads to an eventual reduction of the magnitude of the rarefaction and compression. Hence, the lost work or entropy generation can be considered as the incoherent energy associated with the loss mechanisms. Therefore, distinguishing the incoherent energy from the coherent acoustic energy in each microscopic bin along the wave path would give the total losses in the system. In the above calculations of the exergy flux, it can be noticed that all power terms represent the coherent energy in the system, which means the lost work or entropy generation would be equivalent to the incoherent energy in the system as the lost work is converted to random energy of the gas atoms.

B. Attenuation from the Theory of Continuum Mechanics

For a simple-harmonic plane wave, the viscous loss of energy per unit volume per second can be expressed as[14]

$$\frac{\mathrm{d}\epsilon_{\text{viscous}}}{\mathrm{d}t} = (\eta_{\text{B}} + \frac{4}{3}\mu)\left|\frac{\mathrm{d}u_z}{\mathrm{d}z}\right|^2 = \frac{4}{3}\mu\left|\frac{\mathrm{d}v}{\mathrm{d}z}\right|^2, \tag{15}$$

where $u_z = v$ is the particle velocity in the z-direction, μ is the dynamic viscosity (for argon, $\mu = 22.2 \times 10^{-6}\,\mathrm{Pa \cdot s}$) and η_B is the bulk viscosity of gas (for monatomic gas, $\eta_\mathrm{B} \simeq 0$). The losses due to thermal conduction can be evaluated as[14]

$$\frac{d\epsilon_\mathrm{thermal}}{dt} = \kappa\nabla^2 T = \frac{\kappa}{T}|\nabla T|^2 + T\nabla\,.\,\left(\frac{\kappa}{T}\nabla T\right), \tag{16}$$

where κ is the thermal conductivity and T is the gas temperature. Here T represents the gas temperature in such a way that the magnitude of the temperature fluctuation in the wave would be equivalent to[13]

$$|T - T_\mathrm{eq}| = T_\mathrm{eq}(\gamma - 1)\frac{p_0}{\rho c^2}, \tag{17}$$

where T_eq is the equilibrium temperature of the gas, p_0 is the pressure amplitude of the wave and γ is the specific heat ratio, which is $\frac{5}{3}$ for a monatomic gas such as argon.

In Equation (16), the second term on the right is an oscillatory term whose time average is zero[13]. The T's in the denominator in Equation (16) can be replaced by T_eq to be consistent with linear acoustics[13]. However, in a molecular system, the gas is heated up from its equilibrated temperature (273 K in the case investigated here) during the wave propagation, as shown in Figure 3(a); hence, T_eq was replaced by the mean gas temperature in modeling the simulations here. The thermal losses can then be expressed as

$$\frac{\mathrm{d}\epsilon_\mathrm{thermal}}{\mathrm{d}t} = \frac{\kappa}{T_\mathrm{eq}}|\nabla T|^2. \tag{18}$$

The time-averaged rate of change of the acoustic energy density (rate of energy being lost from the acoustic wave) over the volume can then be estimated as

$$\dot{Q} = \frac{S}{V}\left\langle \int_0^\lambda \left[\frac{\mathrm{d}\epsilon_\mathrm{viscous}}{\mathrm{d}t} + \frac{\mathrm{d}\epsilon_\mathrm{thermal}}{\mathrm{d}t}\right]\mathrm{d}z \right\rangle. \tag{19}$$

The attenuation coefficient for continuum approximations from the simulation results can be evaluated as[14]

$$m_\mathrm{c}^\mathrm{s} = \frac{\dot{Q}}{2I}, \tag{20}$$

where subscripts 'c' and superscript 's' are used to indicate calculation based on continuum mechanics and simulation results, respectively.

Similarly, theoretical approximations of the classical losses based on continuum mechanics are given by[13,14]

$$\frac{\mathrm{d}\epsilon_\mathrm{viscous}}{\mathrm{d}t} = \frac{4}{3}\mu|k v_\mathrm{rms}|^2, \tag{21}$$

and

$$\frac{\mathrm{d}\epsilon_{\mathrm{thermal}}}{\mathrm{d}t} = (\gamma - 1)\frac{\kappa}{c_p}|kv_{\mathrm{rms}}|^2, \tag{22}$$

where c_{p} is the heat capacity at constant pressure (for argon, $c_{\mathrm{p}} = 520.33\,\mathrm{J\,kg^{-1}\,K}$), k $(=\frac{\omega}{c})$ is the wavenumber and v_{rms} is the root-mean-square of acoustic velocity amplitude, which is equivalent to $\frac{1}{\sqrt{2}}\times$ the velocity amplitude v_0 for sinusoidal motion, which is used in this simulation. The continuum approximation of the classical attenuation coefficient results from letting $v_{\mathrm{rms}} = \frac{1}{\sqrt{2}}v_0$ and $I = \frac{1}{2}\rho c v_0^2$ in Equation (20):

$$m_{\mathrm{c}}^{\mathrm{t}} = \frac{2}{3}\mu\frac{k^2}{\rho c} + \frac{1}{2}\frac{\kappa}{c_p}(\gamma - 1)\frac{k^2}{\rho c}, \tag{23}$$

where subscript 'c' and superscript 't' are used to indicate calculation based on continuum mechanics and theoretical approximations.

The classical attenuation coefficient can also be calculated from the complex wavenumber k_c derived for plane wave propagation from the linearized wave equation. The complex wavenumber can be written as[17,19]

$$k_c = \frac{\omega}{c}\left[1 + i\frac{\omega\nu}{c^2}\left(\frac{4}{3} + \frac{\gamma - 1}{Pr}\right)\right]^{-1/2} = k - im, \tag{24}$$

where ν $(=\frac{\mu}{\rho})$ is the kinematic viscosity, Pr $(=\frac{\mu c_p}{\kappa})$ is the Prandtl number, $k(=\frac{\omega}{c})$ is the classical wavenumber and m represents the attenuation rate of the acoustic field by the effects of viscous and thermal conductivity. It can be shown that Equation (24) can be approximated for low frequencies to give an attenuation coefficient consistent with the continuum approximation of the classical attenuation coefficient $m_{\mathrm{c}}^{\mathrm{t}}$ in Equation (23). The attenuation constant calculated from the complex wavenumber k_c using the relation in Equation (24) is denoted by $m_{\mathrm{c_L}}^{\mathrm{t}}$ where subscript '$\mathrm{c_L}$' indicates the evaluation of the attenuation coefficient without an approximation for low frequencies.

C. Standing Wave Theory

In the simulations presented in this paper, the wall oscillates harmonically in the z-direction, with displacement Z_{w} and oscillation speed V_{w}, as a function of time t according to

$$Z_{\mathrm{w}}(t) = a(1 - \cos\omega t), \tag{25}$$

$$V_{\mathrm{w}}(t) = a\omega\sin\omega t, \tag{26}$$

where the displacement and motion of the wall is characterized by the amplitude a and the angular frequency ω. The sound source yields a plane sound wave propagating in the z-direction, leading to a velocity variation

$$v_{\mathrm{i}}(z,t) = v_0 \exp\left[i(\omega t - kz) - mz\right], \tag{27}$$

with a maximum gas velocity $a\omega$, which corresponds to the peak velocity of the oscillating wall, $v_0(= a\omega)$. Due to the specular wall at the far end of the domain, the propagating wave is reflected at the termination, thus giving a backward propagating wave with velocity equal to

$$v_{\mathrm{r}}(z,t) = -v_0 \exp\left[i(\omega t - k(2L_{\mathrm{z}} - z)) - m(2L_{\mathrm{z}} - z)\right]. \tag{28}$$

Superposition of the incident and reflected waves leads to a standing wave of the form[8,28]

$$v(z,t) = A(z)\ \sin\omega t + B(z)\ \cos\omega t, \tag{29}$$

where

$$A(z) = v_0\left[e^{-mz}\ \cos kz\ -\ e^{-m(2L_{\mathrm{z}}-z)}\ \cos k(2L_{\mathrm{z}} - z)\right], \tag{30}$$

$$B(z) = -v_0\left[e^{-mz} \sin kz\ -\ e^{-m(2L_{\mathrm{z}}-z)}\ \sin k(2L_{\mathrm{z}} - z)\right]. \tag{31}$$

$A(z)$ and $B(z)$ are the components of the velocity amplitude of the standing wave, which can be extracted from the numerical solution based on a method used by Hadjiconstantinou and Garcia[8]. A non-linear fit of Equations (30) and (31) to the numerical solution of $A(z)$ and $B(z)$ was performed using the Nelder-Mead simplex method[8,29] to estimate the wavenumber k and the attenuation coefficient m. A phase shift was included in the wave equations for the parameter fits for theoretical prediction at high frequencies in the GHz range due to the entrance effects near to the sound source[8].

IV. RESULTS AND DISCUSSION

A. Steady State Condition during Wave Propagation

The system was monitored to check the variation of the temperature and pressure of the gas during steady-state wave propagation. It was observed that the variation in the mean temperature and pressure of the gas due to dissipation shown in Figure 3 was less than 5% of the gas equilibrium temperature at 273 K and pressure at 1 atm, respectively. Hence the

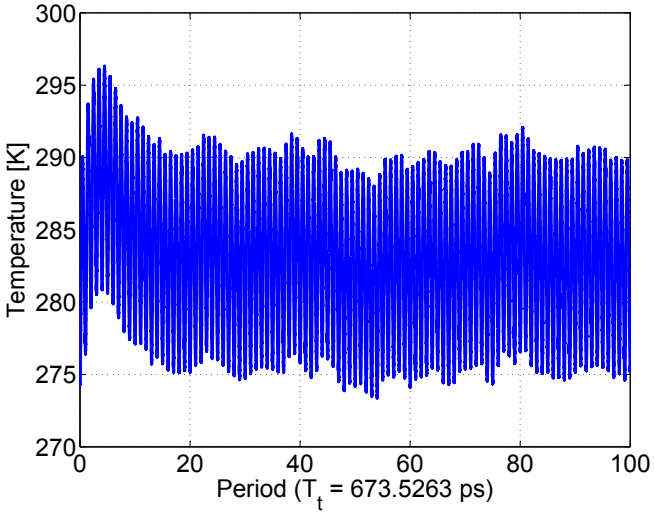

(a)

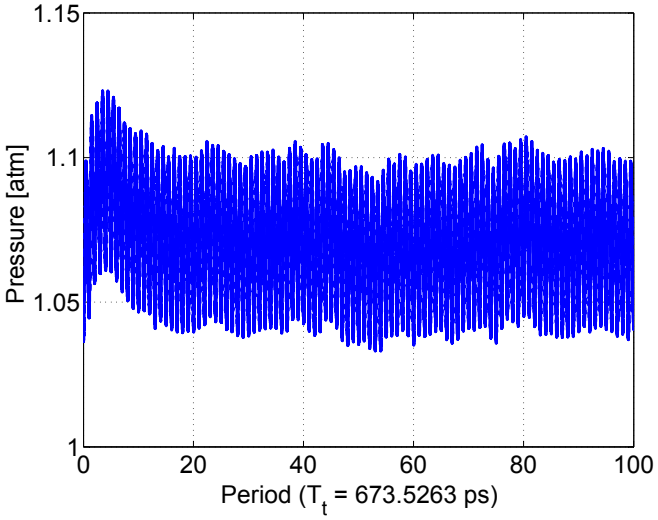

(b)

FIG. 3. Variation of mean spatial temperature (a) and pressure (b) of the gas for a simulation of acoustic wave propagation at frequency $f \approx 1.5\,\mathrm{GHz}$.

change in sound speed[8] (which is proportional to $\sqrt{T}$ or $\sqrt{P}$) would be within 2.5%. The temperature and pressure of the gas fluctuates harmonically due to the oscillation of the piston.

The energy balance of the system was investigated to ensure consistency between the energy input, the energy stored, and the energy dissipated. The acoustic energy input into the system is equivalent to the work done by the piston, which can be calculated from

the recorded normal force on the gas and the oscillating displacement of the piston. The energy extracted by the thermostat was recorded during the simulations, which can also be estimated by subtracting the sum of recorded kinetic and potential energy of interaction of the gas and piston wall from the recorded system's total combined energy. A comparison of the work done and the energy extracted by the thermostat as a function of time (in wave periods) is shown in Figure 4. It can be seen that the two curves are almost identical, indicating the energy input to the system by each oscillation of the wave cycle is extracted by the thermostat. A linear fit of these curves reveals that the amount of energy input to and extracted from the system per period is 511 kcal/mol.

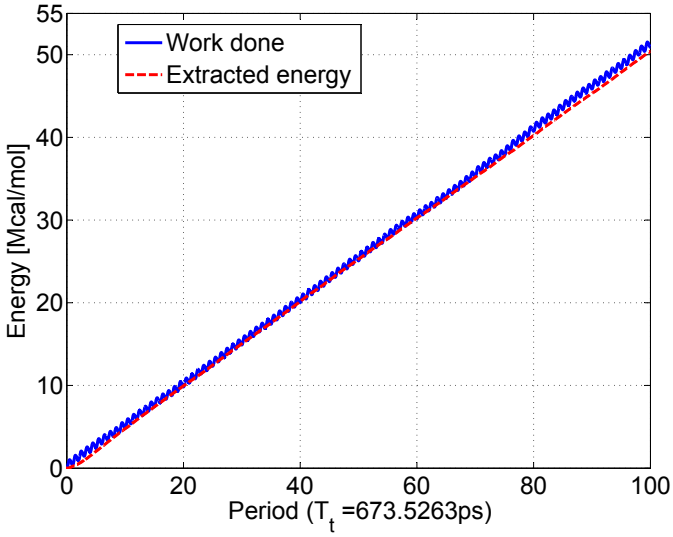

FIG. 4. Work done on the gas by the piston and energy extracted ($= E_{\text{sys}}^{\text{record}} - E_{\text{k}}^{\text{wall \& gas}} - E_{\text{p}}^{\text{wall \& gas}}$) by the thermostat as a function of time during acoustic wave propagation for a wave frequency $f \approx 1.5\,\text{GHz}$.

B. Attenuation of Sound in the Fluid Medium

The dissipation of acoustic power was estimated from the MD simulation data using the concepts of total power and exergy demonstrated by Swift[15,24]. The method is described in Section III A, which was used to calculate acoustic losses and sound attenuation coefficients from a thermostatted MD simulation of acoustic wave propagation. The results are also compared with the continuum approach of predicting the attenuation coefficient and

nonlinear fitting of the waveforms using plane standing wave theory described in Sections III B and III C, respectively.

In order to calculate the losses, acoustic variables such as the sound pressure and particle velocity of the standing wave at different positions along the simulation domain were estimated using the Fourier transform of the time domain data for these variables. Figure 5(a) and 5(b) display the half-wavelength standing wave pattern of the sound pressure and particle velocity for a sound wave frequency $f \approx 1.5\,\mathrm{GHz}$ ($R = 1$). The kinetic energy and potential energy of the gas and the PV term were similarly computed directly from the simulation.

The estimates of acoustic variables can be used to compute the acoustic power $\dot{E}$, total power $\dot{H}$ and exergy flux $\dot{X}$ for the simulation domain using Equations (6), (1) and (10), respectively. Acoustic energy losses in the simulation domain based on the exergy were then evaluated using Equation (13). Thereafter the attenuation was estimated using Equation (14). In the current simulation domain, there was no solid to induce heat conduction in the system. Hence $A_{\mathrm{solid}}\kappa_{\mathrm{solid}}\frac{dT}{dz} \approx 0$ in Equation (1). Furthermore, the thermostat merely extracted excess energy from the system at each cycle of the wave and did not contribute to the power balance of a thermoacoustic system for each period of the wave propagation. Therefore, the elimination of the heat term $\dot{Q}_0$ in Equation (8) is justified, in which the thermostat was accounted for the thermal bath by the term $\dot{Q}_0$ in Equations (4) and (5). Figure 6 shows the estimates of acoustic power $\dot{E}$, total power $\dot{H}$ and exergy flux $\dot{X}$ for the simulation domain. As shown in Figure 6(a), total power consists of a combination of energy fluxes, whereas the exergy flux exhibited in Figure 6(b) represents the associated power available to do work in the presence of a thermostat at temperature $T_0 = 273\,\mathrm{K}$. Thus, as the wave propagates, the work done due to viscous shear across the cross section and the heat conduction between adjacent portions of the medium reduces the power available to do work, which results in generation of entropy. This entropy can be thought of as lost work or the dissipation of acoustic energy in this case. Similarly, the acoustic losses and attenuation coefficient from the simulation results based on continuum mechanics can be evaluated using Equations (19) and (20). The values of the attenuation coefficient using theoretical approximations of classical losses based on continuum mechanics and the linearized wave equation can be calculated from Equations (23) and (24). The non-linear fits (see Appendix) of the acoustic waveforms to the simulated particle velocity amplitude shown in Figure 10

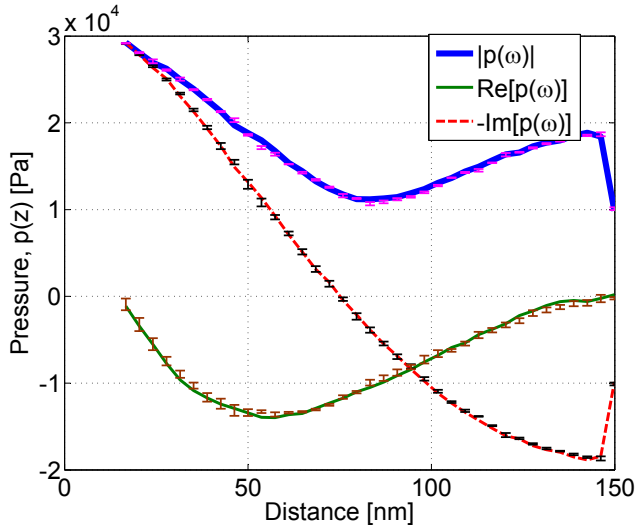

(a)

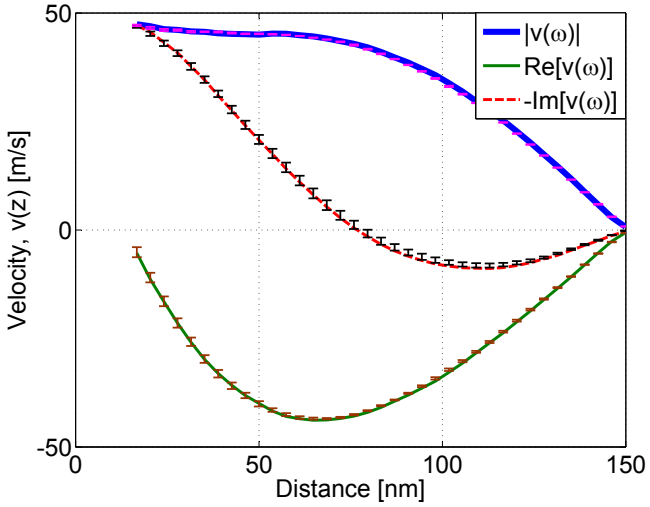

(b)

FIG. 5. Real and imaginary components of acoustic pressure (a) and particle velocity (b) of acoustic wave propagation at frequency $f \approx 1.5\,\mathrm{GHz}$ ($R = 1$). The minimum distance at which points (6 nm) values are displayed is the maximum distance travelled by the piston. Error bars in the figure represent standard deviation in the estimated values of particle velocity and acoustic pressure. The standard errors were calculated using block averages[30,31].

can be used to predict the attenuation coefficient using plane wave theory.

A comparison of the attenuation coefficients estimated from the MD simulation results (based on the exergy and continuum mechanics) and theoretical predictions (from continuum

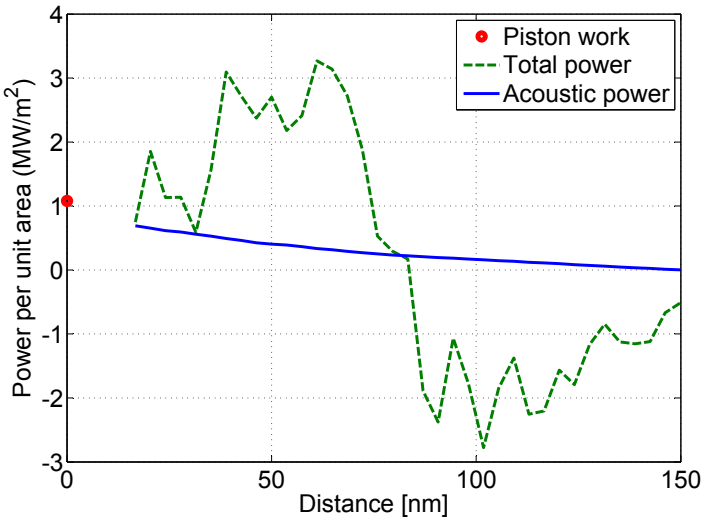

(a)

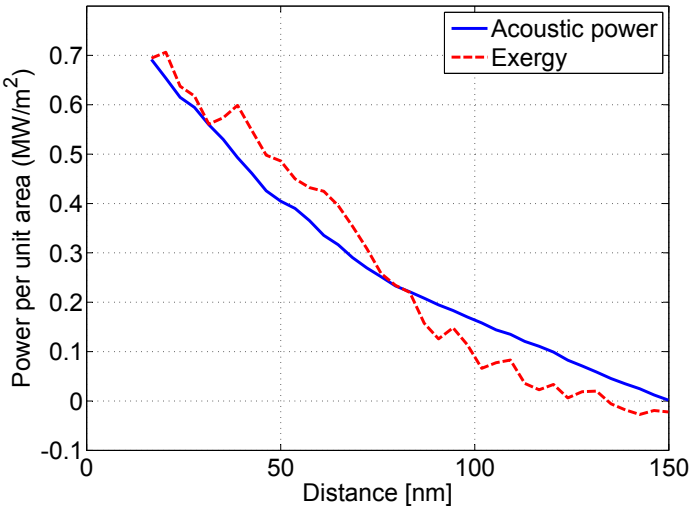

(b)

FIG. 6. Comparison of acoustic power with total power [Equation (1)] (a) and exergy [Equation (10)] (b) for an acoustic domain for acoustic excitation at frequency $f \approx 1.5\,\mathrm{GHz}$ ($R = 1$). Here, the piston work represents the amount of the work done on the gas by the piston, which is equivalent to the acoustic energy input into the system.

approximations and the complex wavenumber) is presented in Table I. The attenuation coefficients were calculated for three different frequencies corresponding to the acoustic Reynolds numbers $R = c^2\rho/\omega\mu$ =1, 0.75, and 0.5. It can be seen that the attenuation coefficient estimated from the MD simulation results based on the exergy (m_e) matches well with the

TABLE I. Comparison of theoretical predictions and simulation results of classical attenuation constant for three different frequencies simulated in this study. The attenuation coefficient values were also compared with different calculation methods of acoustic losses. Here, superscripts 's' and 't' and subscripts 'e', 'f', 'c' and 'c_L' indicate simulation results, theoretical values, exergy concepts, nonlinear fitting using standing wave theory, continuum mechanics, and continuum mechanics without the low-frequency approximation, respectively. Here, a constant value of the sound speed c =460 m s^{-1} was used for these estimates of the attenuation coefficient for all three frequencies. The mean temperatures of the gas for steady-state acoustic wave propagation were 284 K, 280 K and 279 K for wave frequencies of $f \approx 1.5$ GHz, 2.0 GHz, and 2.5 GHz, respectively. These temperatures were used as T_{eq} in Equation (18).

	Acoustic Reynolds Number		
Approach	$R = 1$	$R = 0.75$	$R = 0.5$
	[$f \approx 1.5$ GHz]	[$f \approx 2.0$ GHz]	[$f \approx 2.5$ GHz]
MD results:			
m_{e} $\times 10^7$ (m^{-1})*	0.98	1.14	2.58
$m_{\mathrm{f}}^{\mathrm{s}}$ $\times 10^7$ (m^{-1})† [z>0.5λ_{mfp}]	0.96	1.05	1.40
$m_{\mathrm{f}}^{\mathrm{s}}$ $\times 10^7$ (m^{-1})† [z>λ_{mfp}]	0.97	1.10	1.51
$m_{\mathrm{c}}^{\mathrm{s}}$ $\times 10^7$ (m^{-1})‡	1.94	1.78	2.64
$\frac{m_{\mathrm{e}}}{f^2}$ $\times 10^{-12}$ (Np s^{2}m^{-12})	4.49	2.90	3.91
$\frac{m_{\mathrm{c}}^{\mathrm{s}}}{f^2}$ $\times 10^{-12}$ (Np s^{2}m^{-12})	8.80	4.52	3.99
Theoretical predictions:			
$m_{\mathrm{c}}^{\mathrm{t}}$ $\times 10^7$ (m^{-1})$^\$$	1.25	2.23	3.76
$m_{\mathrm{c_L}}^{\mathrm{t}}$ $\times 10^7$ (m^{-1})§	0.69	0.96	1.23
$\frac{m_{\mathrm{c}}^{\mathrm{t}}}{f^2}$ $\times 10^{-12}$ (Np s^{2}m^{-1})	5.69	5.69	5.69
$\frac{m_{\mathrm{c_L}}^{\mathrm{t}}}{f^2}$ $\times 10^{-12}$ (Np s^{2}m^{-1})	3.14	2.44	1.86

From Equations *(14), †(29), ‡(20), $^\$$(23),§(24)

theoretical predictions ($m_{\mathrm{c_L}}^{\mathrm{t}}$) from the complex wavenumber without low-frequency approximations and the predictions ($m_{\mathrm{f}}^{\mathrm{s}}$) from non-linear fits of the waveforms for each of the three simulated frequencies. The attenuation coefficient ($m_{\mathrm{c}}^{\mathrm{s}}$) for the MD simulation results were also evaluated using the equations of continuum mechanics for viscous and thermal losses

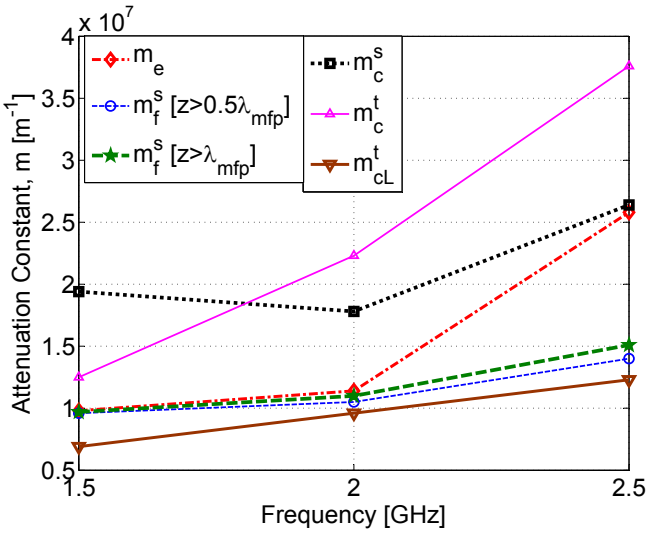

FIG. 7. Comparison of attenuation constant estimates obtained from MD simulation results with those of the theoretical predictions. The solid lines represent the theoretical predictions using the continuum approximations (with $\triangle$) and the complex wavenumber (bold with $\triangledown$), the dotted line (with $\square$) represents the estimate from the MD simulation results evaluated using the continuum approximations, the dashed lines are for the estimates from the MD simulation results evaluated using non-linear fits of the waveforms within domain length $z{>}0.5\lambda_{\mathrm{mfp}}$ (with $\bigcirc$) and $z{>}\lambda_{\mathrm{mfp}}$ (with $\star$) and the dash-dotted line (with $\diamond$) corresponds to the estimate from the MD simulation results based on the exergy.

and compared with the theoretical predictions ($m_{\mathrm{c}}^{\mathrm{t}}$) of the continuum approximations of the equations of classical absorption. Again, the estimates of the attenuation coefficient give consistent agreement between the simulation results and theoretical predictions. However, the theoretical predictions of the attenuation coefficient using the continuum approximations of classical absorption ($m_{\mathrm{c}}^{\mathrm{t}}$) and the estimates of attenuation coefficient based on the exergy (m_{e}) do not agree well. The results in Table I have been plotted in Figure 7 for ease of comparison of the attenuation constant estimates using the various methods. Figure 7 clearly shows that the approximations ($m_{\mathrm{c}}^{\mathrm{s}}$ and $m_{\mathrm{c}}^{\mathrm{t}}$) based on continuum theory fails to match the estimates of the attenuation constant obtained using the exergy (m_{e}) and nonlinear fitting ($m_{\mathrm{f}}^{\mathrm{s}}$) of the MD simulation results for the frequencies simulated in this study. On the other hand, the estimates ($m_{\mathrm{c_L}}^{\mathrm{t}}$) based on the complex wavenumber match closely to those of both the nonlinear fitting and exergy concept. The approximation ($m_{\mathrm{c}}^{\mathrm{t}}$) of continuum theory over-

estimates of the attenuation coefficient compared with both the simulation results (m_{e}) and the predictions ($m_{\mathrm{c_L}}^{\mathrm{t}}$) from the complex number without low-frequency approximations.The discrepancies between these quantities can be explained by the range of validity of the continuum theory for predictions of the attenuation coefficient. The validity of the continuum theory is defined by the relaxation time for viscous and thermal absorptions. The relaxation times for viscous and thermal conduction in fluid are[13]

$$\tau_S = \frac{4}{3}\frac{\mu}{\rho c^2}, \tag{32}$$

and

$$\tau_\kappa = \frac{1}{\rho c^2}\frac{\kappa}{c_p}, \tag{33}$$

respectively. To comply with the assumptions in the continuum theory for the fluid continuum, the wave frequency, f, should be much smaller than the relaxation frequencies f_S and f_κ, for viscous and thermal absorptions, respectively[13]. Thus, the continuum theory should only be valid for values of the dimensionless coefficient $\omega\tau_{S/\kappa}$ much smaller than unity[13]. The dimensionless coefficient calculated for each frequency is listed in Table II and can be seen to be order of 1, thus violating the continuum theory. Furthermore, Greenspan's experimental data[19,32] for sound wave propagation in a monatomic gas show that the continuum theory is valid only if $\frac{\rho c^2}{\omega\mu\gamma}$ is greater than 10. The values of parameter $\frac{\rho c^2}{\omega\mu\gamma}$ for each of the simulated frequencies is given in Table II and can be seen to be much smaller than 10, confirming again that the continuum theory is not applicable to the conditions simulated for computing the approximations of classical absorption. Hence, it can be concluded that discrepancies in the attenuation coefficients are expected.

It can also be seen that the attenuation coefficient increases as the Reynold's number decreases. This indicates that classical losses (attenuation) increase with the wave frequency. The changes in the attenuation coefficient with frequency also demonstrates that the MD method can simulate classical absorption due to viscous and thermal losses in a fluid medium and can also simulate the change in the effects of classical absorption due to a change in frequency.

Furthermore, previous experimental investigations have shown that the attenuation coefficient varies with the wave frequency and is proportional to the square of the frequency[13]. Therefore, attenuation data are usually presented as a function of $\frac{m}{f^2}$ in experimental measurements of attenuation and plotted against the wave frequency f to demonstrate any

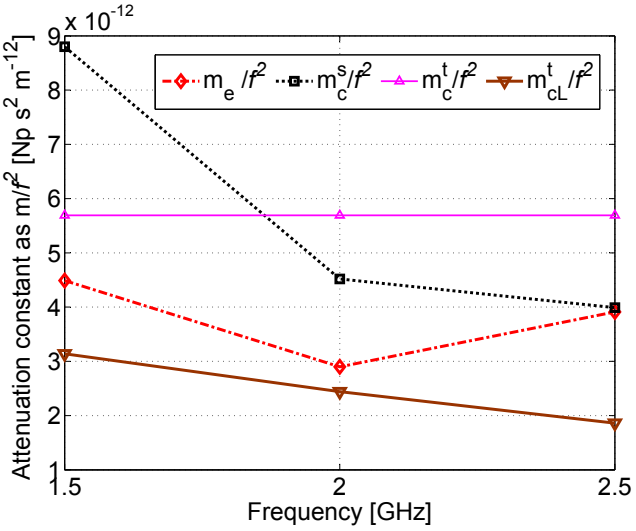

FIG. 8. Comparison of attenuation constant estimates as a function of $\frac{m}{f^2}$ obtained from MD simulation results with those of the theoretical predictions. The solid lines represent the theoretical predictions using the continuum approximations ($\triangle$) and the complex wavenumber (bold with $\triangledown$), the dotted line (with $\square$) represents the estimate from the MD simulation results evaluated using the continuum approximations, and the dash-dotted line (with $\diamond$) corresponds to the estimate from the MD simulation results based on the exergy.

departure from a linear relationship, which indicates deviations from the predictions of continuum (or classical) theory[13]. A list of the calculated values of $\frac{m}{f^2}$ from the MD simulation results is included in Table I and is plotted in Figure 8. It can be observed that the value of the attenuation coefficients in the form of $\frac{m}{f^2}$ gives a constant value of $5.69 \times 10^{-12}\,\mathrm{Np\,s^2m^{-1}}$ for the theoretical prediction using continuum approximations, whereas the value of $\frac{m}{f^2}$ decreases with increasing acoustic frequency when the calculations were performed without the approximation for low frequency. The simulation results for this value of $\frac{m}{f^2}$ estimated based on the exergy and continuum equations similarly indicate a departure from constancy, implying deviation from the continuum theory. As shown in Figures 7 and 8, these discrepancies are expected given that the simulated acoustic waves are in the transition flow regime ($0.1<Kn<10$), which represents the transition between diffusive (continuum) and ballistic (free molecular flow) molecular behavior[8,9], based on their corresponding Knudsen numbers, $Kn \approx 0.25$, 0.34, and 0.42 for frequencies of $f \approx 1.5$, 2 and 2.5 GHz, respectively. It can also be observed from Figure 7 that the discrepancy increases with frequency as the

TABLE II. Comparison of relaxation frequency for viscous (f_S) and thermal (f_κ) absorptions with wave frequencies (f). The dimensionless coefficients $\omega\tau_S$ and $\omega\tau_\kappa$ are also evaluated for each of the wave frequencies along with Greenspan's[32] validity parameter $\frac{\rho c^2}{\omega\mu\gamma}$.

Reynolds number	f_S (GHz)	f_κ (GHz)	$\omega\tau_S$	$\omega\tau_\kappa$	$\frac{\rho c^2}{\omega\mu\gamma}$
R=1 [$f \approx 1.5\,\text{GHz}$]	13.02	11.96	0.72	0.78	1.12
R=0.75 [$f \approx 2.0\,\text{GHz}$]	-	-	0.96	1.04	0.84
R=0.5 [$f \approx 2.5\,\text{GHz}$]	-	-	1.24	1.35	0.64

Knudsen number becomes greater and the system moves further away from the range of validity of continuum mechanics. Thus, the simulation results confirm the deviation from the continuum theory for the attenuation coefficients at the high frequencies simulated in this study. Consequently, it confirms that the developed framework provides a numerical method for simulating classical losses in a regime where continuum approaches are not applicable, which will be the case for an acoustic wave in the audible frequency range interacting with nanoscale structures or pores.

As demonstrated earlier, at high frequencies the classical results of continuum theory are no longer accurate. However, higher-order approximation of the Boltzmann Transport Equations such as Burnett or n-Moment equations are useful to qualitatively describe the acoustic absorption mechanisms at higher frequencies[8,32]. The MD simulation results were also compared with the experimental data of Greenspan[32] and the theoretical predictions of the Burnett and super-Burnett theories and the 8- and 11-moment results of Sirovich and Thurber[33] as shown in Figure 9. It can be observed that the MD results are qualitatively consistent with the experimental data and the theoretical predictions, but predict a higher absorption coefficient at higher frequencies (i.e. at lower Reynold's number). This confirms that the MD simulation model can capture the behavior consistently and is expected to provide better agreement with experiment at lower frequencies.

Overall, the MD simulation platform and analysis framework presented in the current work is an important foundation for investigating nanoscale effects on sound propagation and absorption. The developed methodology can be straightforwardly extended to systems in which an acoustic wave interacts with a nanomaterial such as a carbon nanotube. To

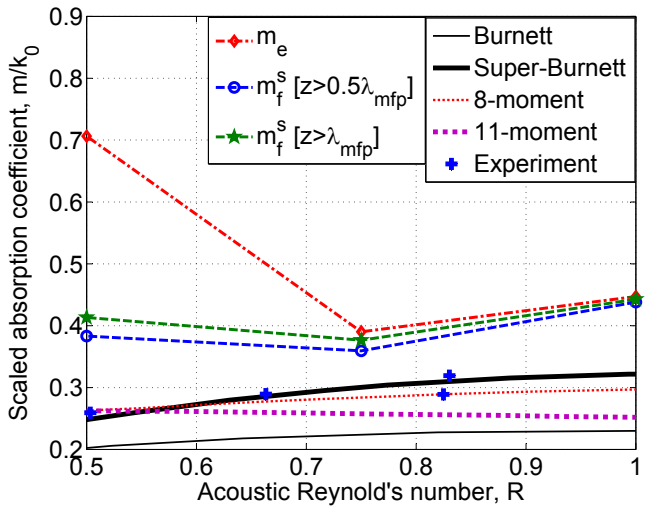

FIG. 9. Scaled absorption coefficient $\frac{m}{k_0}$ versus acoustic Reynolds number (R). The experimental data (+) of Greenspan[32] and the theoretical predictions of Burnett (solid line), super-Burnett (bold solid line), and the 8- (dotted line) and 11-moment (bold-dotted line) solutions were reproduced from the study by Hadjiconstantinou and Garcia[8].

permit the study of acoustic wave propagation in the audible frequency range (0.02 - 20 kHz) simulations would need to be extended to the millisecond time scale, which would require considerable computational resources[34].

V. CONCLUSION

This paper presented the study of sound attenuation in high-frequency acoustic wave propagation using a molecular dynamics simulation. An analytical method was demonstrated for analyzing the sound attenuation induced due to classical (thermal and viscous) losses in a thermostatted molecular dynamics (MD) simulation of high-frequency wave propagation in a simple gas, in which the coherent acoustic energy is transferred to random energy of atoms via the stochastic nature of interactions of atoms as the wave propagates. The classical losses in the acoustic medium (gaseous argon) were quantified and described in terms of attenuation coefficients. The attenuation coefficients were evaluated using the thermodynamic concept of exergy. The attenuation coefficient results were verified against predictions using standing wave theory and theoretical approximations based on continuum mechanics. Estimates of the attenuation coefficient from the simulation data provided

consistent agreement across the three different frequencies studied in this study and gave a good approximation to the predictions using standing wave theory. Calculations of the attenuation coefficients as a function of the squared frequency indicate that the estimates deviate from the predictions of continuum theory for the high-frequency waves simulated in this study. Based on the comparison of the theoretical calculations and MD simulation results, it can be concluded that acoustic absorption effects in a simple fluid can be analyzed using the concept of exergy and the demonstrated method can be extended in the future to investigate the absorption effects of nanomaterials.

ACKNOWLEDGEMENT

This research was supported under Australian Research Council's Discovery Projects funding scheme (project number DP130102832). The assistance of Mr Jesse Coombs with the simulations is greatly appreciated. This work was supported by computational resources provided by eResearchSA.

Appendix A: Prediction of wave parameters - Standing wave theory

The non-linear fitting of the standing wave equations described in Section III C can be used to predict the acoustic parameters such as the sound speed (c) and attenuation coefficient (m) from the wave pattern of the particle velocity. Figure 10 shows the waveforms fitted to the simulation data of the cosine and sine components of the velocity amplitude without any restriction to the zone over which the data is fit. The extracted parameters for the non-linear fitting without any restriction were $c = 435\,\mathrm{m\,s^{-1}}$ and $m = 0.914 \times 10^7\,\mathrm{m^{-1}}$. It can be seen that the fitting of the waveforms deteriorates near to the reflective wall. Consequently, if the fitting is restricted outside half a mean free path ($\lambda_{\mathrm{mfp}} = M_{\mathrm{m}}/\sqrt{2}\pi\sigma^2\rho$ $= 7.28 \times 10^{-8}$ m) or one mean free path from the sound source, the waveforms give good fits of the velocity components. However, the waveforms give the best fit of the curve for the domain length $z{>}\lambda_{\mathrm{mfp}}$ by a constant sound speed $c = 447\,\mathrm{m\,s^{-1}}$ and attenuation coefficient $m = 0.967 \times 10^7\,\mathrm{m^{-1}}$. On the other hand, the fit deteriorates very quickly in the region $0{<}z{<}\lambda_{\mathrm{mfp}}$. These can be attributed to the effect of free molecular flow near the source which may be important at this frequency[8,11].

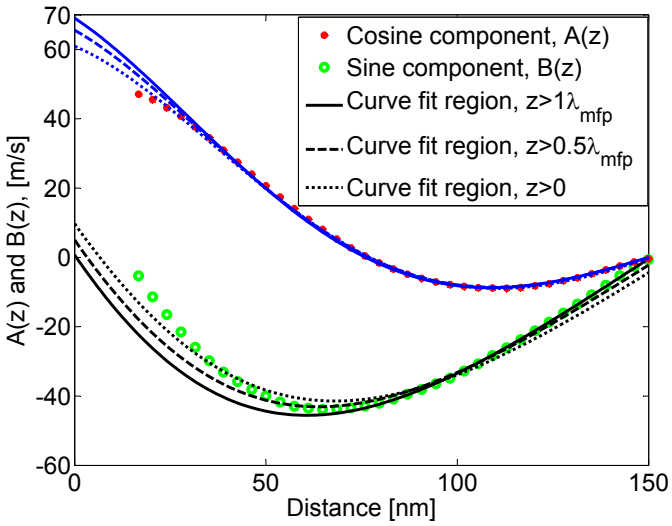

FIG. 10. Non-linear curve fit to cosine and sine components, $A(z)$ and $B(z)$, of the velocity amplitude as a function of distance for acoustic wave frequency $f \approx 1.5\,\mathrm{GHz}$ ($R = 1$). The curve fitting was applied in the regions of the domain length $z{>}0$, $z{>}0.5\lambda_{\mathrm{mfp}}$ and $z{>}\lambda_{\mathrm{mfp}}$. The predicted values for each of these fits are: $c = 435\,\mathrm{m\,s^{-1}}$ and $m = 0.914 \times 10^7\,\mathrm{m^{-1}}$, $c = 442\,\mathrm{m\,s^{-1}}$ and $m = 0.957 \times 10^7\,\mathrm{m^{-1}}$, and $c = 447\,\mathrm{m\,s^{-1}}$ and $m = 0.967 \times 10^7\,\mathrm{m^{-1}}$, respectively.

REFERENCES

[1]M. Ayub, A. Zander, C. Howard, B. Cazzolato, D. Huang, V. Shanov, and N. Alvarez, "Normal incidence acoustic absorption characteristics of a carbon nanotube forest," Appl. Acoust. **127**, 223–229 (2017).

[2]M. Ayub, A. C. Zander, C. Q. Howard, B. S. Cazzolato, D. M. Huang, V. N. Shanov, and N. T. Alvarez, "Acoustic absorption behaviour of a tall carbon nanotube forest," in *Proc. Acoust. 2016* (Brisbane, Australia, 2016) pp. 1–10.

[3]M. Ayub, A. C. Zander, C. Q. Howard, B. S. Cazzolato, V. N. Shanov, N. T. Alvarez, and D. M. Huang, "Acoustic absorption behavior of carbon nanotube arrays," in *43rd Int. Cong. Noise Control Eng. (Inter-Noise 2014)*, Vol. 249 (2014) pp. 929–938.

[4]M. Bandarian, A. Shojaei, and A. M. Rashidi, "Thermal, mechanical and acoustic damping properties of flexible open-cell polyurethane/multi-walled carbon nanotube foams: effect of surface functionality of nanotubes," Polym. Int. **60**, 475–482 (2011).

[5]R. Verdejo, R. Stmpfli, M. Alvarez-Lainez, S. Mourad, M. Rodriguez-Perez, P. Brhwiler, and M. Shaffer, "Enhanced acoustic damping in flexible polyurethane foams filled with

carbon nanotubes," Compos. Sci. Technol. **69**, 1564 – 1569 (2009).

[6]S. Basirjafari, R. Malekfar, and S. E. Khadem, "Low loading of carbon nanotubes to enhance acoustical properties of poly(ether)urethane foams," J. Appl. Phys. **112 (10)**, 104312: 1–8 (2012), https://doi.org/10.1063/1.4765726.

[7]Y. J. Qian, D. Y. Kong, Y. Liu, S. M. Liu, Z. B. Li, D. S. Shao, and S. M. Sun, "Improvement of sound absorption characteristics under low frequency for micro-perforated panel absorbers using super-aligned carbon nanotube arrays," Appl. Acoust. **82**, 23 – 27 (2014).

[8]N. G. Hadjiconstantinou and A. L. Garcia, "Molecular simulations of sound wave propagation in simple gases," Phys. Fluids **13**, 1040–1046 (2001).

[9]N. G. Hadjiconstantinou, "Sound wave propagation in transition-regime micro- and nanochannels," Phys. Fluids **14**, 802–809 (2002).

[10]M. Ayub, A. C. Zander, C. Q. Howard, and B. S. Cazzolato, "A review of acoustic absorption mechanisms of nanoscopic fibres," in *Proc. Acoust. 2011* (Gold Coast, Australia, 2011) pp. 77–84.

[11]M. Ayub, A. C. Zander, C. Q. Howard, D. M. Huang, and B. S. Cazzolato, "Molecular dynamics simulations of sound wave propagation in a gas and thermo-acoustic effects on a carbon nanotube," J. Comput. Acoust. [special issue: 11th Int. Conf. Theor. Comput. Acoust. (ICTCA)] **23**, 1540012:1–18 (2015).

[12]M. Ayub, A. C. Zander, C. Q. Howard, B. S. Cazzolato, and D. M. Huang, "A review of MD simulations of acoustic absorption mechanisms at the nanoscale," in *Proc. Acoust. 2013* (Victor Harbor, Australia, 2013) pp. 19–26.

[13]L. Kinsler, A. Frey, A. Coppens, and J. Sanders, *Fundamentals of Acoustics*, 4th ed. (John Wiley & Sons, Inc., New York, 2000) Chap. 8, Sec. 8.1-8.5, pp. 210–218.

[14]P. M. Morse and K. U. Ingard, *Theoretical Acoustics* (McGraw-Hill, New York, 1968) Chap. 6, Sec. 6.4, pp. 270–277.

[15]G. W. Swift, *Thermoacoustics: A unifying perspective for some engines and refrigerators* (Acoustical Society of America, New York, 2002) Chap. 6, Sec. 6.1-6.2, pp. 147–158.

[16]J. Allard and N. Atalla, *Propagation of Sound in Porous Media: Modelling Sound Absorbing Materials*, 2nd ed. (John Wiley & Sons, Ltd., UK, 2009) Chap. 4, Sec. 4.2-4.3, pp. 45–53.

[17]C. Q. Howard and B. S. Cazzolato, *Acoustic analysis using Matlab and Ansys* (CRC press, 2014).

[18]E. Meyer and E. G. Neumann, *Physical and Applied Acoustics*, Chapter 3 (Academic Press, New York and London, 1972) Chap. 3, Sec. 3.1, pp. 95–102.

[19]A. D. Pierce, *Acoustics: An introduction to its physical principles and applications* (Acoustical Society of America, New York, 1989) Chap. 10, Sec. 10-2, pp. 515–519.

[20]S. Plimpton, "Fast parallel algorithms for short-range molecular dynamics," J. Comput. Phys. **117**, 1–19 (1995).

[21]LAMMPS-Manual, *LAMMPS Users Manual*, Sandia National Laboratories (2013).

[22]C. F. Carlborg, J. Shiomi, and S. Maruyama, "Thermal boundary resistance between single-walled carbon nanotubes and surrounding matrices," Phys. Rev. B **78**, 1–8 (2008).

[23]J. D. Weeks, D. Chandler, and H. C. Andersen, "Role of repulsive forces in determining the equilibrium structure of simple liquids," J. Chem. Phys. **54**, 5237–5247 (1971).

[24]G. W. Swift, *Thermoacoustics: A unifying perspective for some engines and refrigerators* (Acoustical Society of America, New York, 2002) Chap. 5, Sec. 5.2, pp. 128–134.

[25]A. Bejan, *Advanced Engineering Thermodynamics*, second edition ed. (Wiley, New York, 1997).

[26]F. Jacobsen, "Active and reactive, coherent and incoherent sound fields," J. Sound Vib. **130**, 493–507 (1989).

[27]E. Kuipers, *Measuring sound absorption using local field assumptions*, Ph.D. thesis, University of Twente, Enschede, The Netherlands (2013).

[28]R. J. Wang and K. Xu, "The study of sound wave propagation in rarefied gases using unified gas-kinetic scheme," Acta Mech. Sinica **28**, 1022–1029 (2012).

[29]W. H. Press, S. A. Teukolsky, W. T. Vetterling, and B. P. Flannery, *Numerical Recipes in C*, 2nd ed. (Cambridge University Press, Cambridge, 1992).

[30]A. Grossfield and D. M. Zuckerman, "Quantifying uncertainty and sampling quality in biomolecular simulations," Annu. Rep. Comput. Chem. **5**, 23–48 (2009).

[31]D. Frenkel and B. Smit, *Understanding Molecular Simulations: From algorithms to applications* (Academic Press, San Diego, 2002) Chap. 4 (Appn. D), pp. 525–532.

[32]M. Greenspan, "Propagation of sound in five monatomic gases," J. Acoust. Soc. Am. **28**, 644–648 (1956).

[33]L. Sirovich and J. K. Thurber, "Propagation of forced sound waves in rarefied gas dynamics," J. Acoust. Soc. Am. **37 (2)**, 329–339 (1965).

[34]D. E. Shaw, P. Maragakis, K. Lindorff-Larsen, S. Piana, R. O. Dror, M. P. Eastwood, J. A. Bank, J. M. Jumper, J. K. Salmon, Y. Shan, and W. Wriggers, "Atomic-level characterization of the structural dynamics of proteins," Science **330**, 341 – 346 (2010).